

Improving Multi-hop Logical Reasoning in Knowledge Graphs with Context-Aware Query Representation Learning

Jeonghoon Kim¹, Heesoo Jung¹, Hyeju Jang², and Hogun Park^{*1}

¹Sungkyunkwan University, Republic of Korea

²Indiana University Indianapolis, USA

{kjh9503, steve305}@skku.edu, hyejuj@iu.edu, hogunpark@skku.edu

Abstract

Multi-hop logical reasoning on knowledge graphs is a pivotal task in natural language processing, with numerous approaches aiming to answer First-Order Logic (FOL) queries. Recent geometry (e.g., box, cone) and probability (e.g., beta distribution)-based methodologies have effectively addressed complex FOL queries. However, a common challenge across these methods lies in determining accurate geometric bounds or probability parameters for these queries. The challenge arises because existing methods rely on linear sequential operations within their computation graphs, overlooking the logical structure of the query and the relation-induced information that can be gleaned from the relations of the query, which we call the *context of the query*. To address the problem, we propose a model-agnostic methodology that enhances the effectiveness of existing multi-hop logical reasoning approaches by fully integrating the context of the FOL query graph. Our approach distinctively discerns (1) the structural context inherent to the query structure and (2) the relation-induced context unique to each node in the query graph as delineated in the corresponding knowledge graph. This dual-context paradigm helps nodes within a query graph attain refined internal representations throughout the multi-hop reasoning steps. Through experiments on two datasets, our method consistently enhances the three multi-hop reasoning foundation models, achieving performance improvements of up to 19.5%. Our code is available at <https://github.com/kjh9503/caqr>.

1 Introduction

Multi-hop logical reasoning on Knowledge Graphs (KGs) is a crucial task in natural language processing. KGs, which map real-world knowledge as interconnected entities and relationships (Sinha et al., 2015; Vrandečić and Krötzsch, 2014), help

*Corresponding Author

Q : What are the names of the teams playing the team sports featured in the 1980 Olympics?

FOL : $q = A. \exists V: \text{FeaturedAt}^{-1}(1980 \text{ Olympic}, V) \wedge \text{TeamPlays}^{-1}(V, A)$

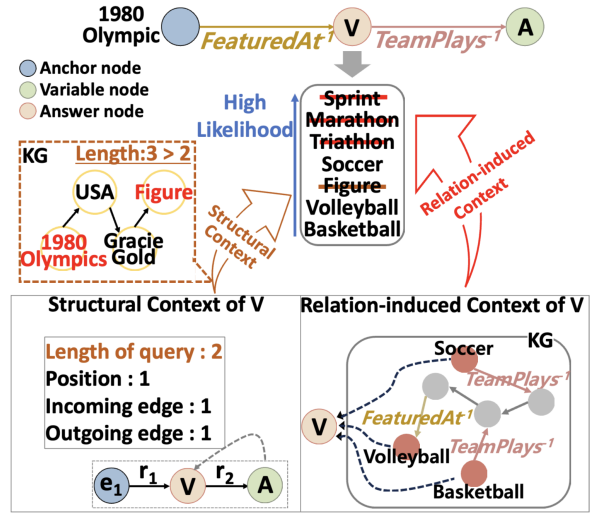


Figure 1: The existing methods may include wrong answers such as, *Sprint*, *Marathon*, *Triathlon*, and *Figure* because the candidates held by the variable node (V) in the inference process are only influenced by the *1980 Olympic* and *FeaturedAt⁻¹*. However, our approach uses structural and relation-induced contexts to find a more accurate embedding of V, which helps us to predict answers that are close to the ground truth.

answer complex questions expressed as First-Order Logic (FOL) queries. A FOL query can be converted into a computation graph, using variables, conjunctions, and existential quantification operators to represent a natural language question. For example, the computation graph of the query representing “What are the names of the teams playing the team sports featured in the 1980 Olympics?” can be constructed with two conjunction relations: 1) finding the sports featured in the 1980 Olympics, and 2) finding the sports teams that play that sports (see Figure 1 for illustration).

Recent advancements in multi-hop reasoning leverage the power of embedding-based models such as Q2B (Ren et al., 2020), BetaE (Ren and

Leskovec, 2020), and ConE (Zhang et al., 2021). These models embed both a given query and entities (answer candidates) in a KG into a latent space. In this space, entities relevant to the query are positioned closer to the query’s embedding. This allows the model to predict the answer to the query by identifying these nearby entities.

Despite their success, these embedding-based models still face a major hurdle: learning more accurate geometric bounds or probability parameters for complex queries. Prior models handle all queries in the same way, building the embedding for each relationship (e.g., *FeaturedAt*⁻¹ or *TeamsPlay*⁻¹ in Figure 1) one after another. This approach overlooks the structural context and relation-induced context within each question. Therefore, entities like *Sprint*, *Marathon*, *Triathlon*, and *Figure* are treated as answers by the existing models (Ren et al., 2020; Ren and Leskovec, 2020; Zhang et al., 2021) based on the given query in Figure 1.

To address this limitation, we propose a novel query embedding technique, named **CaQR** (Context-aware Query Representation learning), that incorporates both *structural context* and *relation-induced context*. The structural context encodes the positional or role-like information of a node within the query computation graph. For example, in Figure 1, the structural context of node V could include the number of incoming and outgoing edges, the canonical position of V within the query graph, and the length of the query graph containing node V. Based on this, *Figure* can be excluded as a V candidate because it is unlikely to be derived through the one-hop reasoning from the *1980 Olympics* in KG. The relation-induced context, on the other hand, leverages KG entities linked to each node’s relations. For instance, in the query graph shown in Figure 1, the relation-induced context—acquired by identifying nodes in the KG associated with *TeamsPlay*⁻¹—suggests that *Sprint*, *Marathon*, and *Triathlon* are not suitable candidates for V by accentuating the entities which linked to the *TeamsPlay*⁻¹ relations (*Soccer*, *Volleyball*, and *Basketball*). By incorporating structural and relation-induced contexts into the existing query embedding methods, our approach mitigates the cascading errors that can arise from the step-by-step computation characteristic of these methods.

Our contributions are threefold: (1) We propose a novel query representation learning method

that leverages two types of context within a query computation graph: structural context and relation-induced context, which are often overlooked in previous methods. (2) Our proposed technique is applicable to any existing query embedding-based method, as it utilizes structural and relation-induced context acquired from the input query graph, irrespective of the models. (3) Our experiments show that our method leads to performance improvements for various models (Q2B (Ren et al., 2020), BetaE (Ren and Leskovec, 2020), and ConE (Zhang et al., 2021)), which have received considerable attention in various FOL tasks as foundation models. Specifically, our experiments on two benchmark datasets demonstrate that our method consistently improves these models, achieving up to a 19.5% enhancement in query reasoning tasks compared to their baselines.

2 Related Work

Geometry-based. These approaches represent each query as a geometric shape in the embedding space. They then identify entities located close to that shape as answers to the query. For instance, GQE (Hamilton et al., 2018) maps entities to points and employs neural networks to model logical operators. Q2B (Ren et al., 2020) and its extension (Liu et al., 2021) use hyper-rectangles, or boxes, to represent queries. These boxes are defined by a center and offset, and entities positioned closer to them are considered potential answers. ConE (Zhang et al., 2021) represents queries using multiple two-dimensional cones characterized by their axis and aperture angle. Similar to Q2B, entities lying closer to the cone representing the query are considered potential answers. However, these geometry-based models fail to harness both structural and relation-induced context information.

Probability-based. In contrast to geometry-based approaches, probability-based methods represent queries as probability distributions. For example, BetaE (Ren and Leskovec, 2020) uses multiple beta distributions to represent a query, entities, and relations. Similar approaches include GammaE (Yang et al., 2022) with gamma distributions and PERM (Choudhary et al., 2021) with multivariate Gaussian distributions. These methods measure the distance between the query embedding and candidate entities using KL-divergence. FuzzQE (Chen et al., 2022b) takes a different approach, mapping queries and entities to a fuzzy

space. It represents the answer set as a fuzzy vector and calculates the probability of an entity being an answer using a score function. Similarly, GNN-QE (Zhu et al., 2022) adopts fuzzy logic to represent queries and entities but uses graph neural networks for projection in an incomplete KG. On the other hand, WFRE (Wang et al., 2023a) models queries and entities as discretized mass vectors that satisfy fuzzy logic. It models logical operators through t-norm or t-conorm functions and measures the distance between mass vectors using the optimal transport theory (Peyré and Cuturi, 2019). While each method has its advantages and disadvantages and is selectively utilized in various FOL-based applications (Tang et al., 2023; Liang et al., 2023; Xiong et al., 2023), the potential of query-based context encoding to enhance multiple multi-hop reasoning approaches and yield robust performance improvements has not received sufficient attention.

Query Encoder-based. There are auxiliary transformation encoders for representing the FOL queries for multi-hop reasoning. These include Q2T (Xu et al., 2023) and LMPNN (Wang et al., 2023b), which take distinct approaches to tackling complex queries. Q2T transforms the complex query into a single virtual triple of head, relation, and tail components. It computes the score of this virtual triple with a pre-trained KG embedding model to predict the answer to the query. LMPNN (Wang et al., 2023b), on the other hand, decomposes the complex multi-hop query into multiple simpler triples. It generates a message using the entity embedding to maximize the score for each triple, utilizing a pre-trained KG embedding model. However, these approaches require initial KG embeddings from extensive pre-training and are not applicable to various multi-hop reasoning approaches.

3 Preliminaries

Given an entity set \mathcal{V} and a relation set \mathcal{R} , the KG $G = (h, r, t) \subset \mathcal{V} \times \mathcal{R} \times \mathcal{V}$ represents a collection of triples that encapsulate factual information in the real world. Here, $h, t \in \mathcal{V}$, and $r \in \mathcal{R}$. When considering each relation as a binary function, such as $r(h, t)$, following the structure of predicate logic, the triples observed from the KG hold a value of *True*.

3.1 First-Order Logic (FOL) Queries

The First-Order Logic (FOL) queries take predicate logic, allowing the use of quantified variables. A FOL query is composed of a non-variable anchor entity set $\mathcal{V}_a \subseteq \mathcal{V}$, an existential quantified set $\{V_1, \dots, V_k\}$ of size k , and a target variable $V_?$, which is an answer to a certain query. For example, in Figure 1, \mathcal{V}_a is $\{1980\text{ Olympic}\}$, the existential quantified set is $\{V\}$, and the target variable is A . Generally, FOL queries include four logical operators: the existential quantifier (\exists), conjunction (\wedge), disjunction (\vee), and negation (\neg). We can formulate a FOL query q as follows:

$$q = V_?. \exists V_1, \dots, V_k : c_1 \vee c_2 \vee \dots \vee c_n. \quad (1)$$

$$c_i = a_{i_1} \wedge a_{i_2} \wedge \dots \wedge a_{i_m}. \quad (2)$$

Each atomic formula a_{i_j} is in the form of predicate logic which has the form of $r(v_a, V)$ or $\neg r(v_a, V)$ or $r(V', V)$ or $\neg r(V', V)$ consisting a conjunction c_i of m predicates. v_a is an element of \mathcal{V}_a . V and V' are elements of $\{V_?, V_1, \dots, V_k\}$ and $\{V_1, \dots, V_k\}$, respectively ($V' \neq V$). Note that we call this atomic formula a_{i_j} a *branch* of a query graph.

3.2 Query Graph

In BetaE (Ren and Leskovec, 2020), FOL query answering tasks are categorized into pre-defined multi-hop reasoning tasks using 14 different query types. Each query type can be represented by a corresponding query graph and all queries can be interpreted as corresponding natural language questions. For instance, a FOL query for “*What are the names of the teams playing the team sports featured in the 1980 Olympics?*” can be represented by the query graph shown in Figure 1. A query graph consists of anchor nodes, variable nodes, and answer nodes. Variable nodes signify entities fulfilling individual sub-conditions within the query, while the answer node represents the entity satisfying the entire query. In Figure 2, you can observe five types of query graphs, and all query types can be found in Appendix A.2.

3.3 Computation Graph

The computation graph details the computation procedure to obtain the embedding of each node in the query graph. In a computation graph, each node represents an embedding of an entity (or a set of entities) in the KG, and each edge signifies a logical

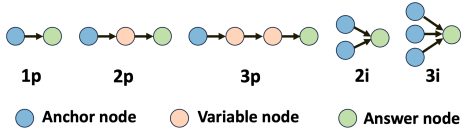


Figure 2: Five types of query graph

transformation (e.g., relational projection, intersection/union/negation operators) of this distribution. The computation graph for a FOL query resembles a tree. The root node of the computation graph represents the answer (or target) variable, with one or more anchor nodes provided by the FOL. Embeddings of entities and transformation operators are initialized; embeddings of anchor nodes are then fed into the neural network of logical operators in a serial manner to obtain the final embeddings for the answer variable, thereby creating a query embedding. During training, models ensure the proximity of query embeddings to the ground truth. In the prediction stage, entities close to the query embedding are utilized for prediction. Further details on the logical operators are included in the Appendix B.

4 Methodology

In this section, we explain CaQR, our method that leverages context information from the query graph to create more accurate and nuanced entity embeddings. By incorporating context, CaQR can make fine-grained adjustments within the embedding space, capturing the complexities of real-world queries.

CaQR concentrates on two key types of context: *structural context* and *relation-induced context*. The structural context combines positional cues (where nodes appear in the query) and functional roles (the specific role a node plays) to comprehend the overall structure and relationships within the query. Furthermore, the relation-induced context focuses on the specific relationships and interactions between entities within the query. CaQR combines these structural and relation-induced contexts to create a more comprehensive query embedding.

4.1 Learning Structural Context

To capture structural context, we propose using position embeddings, role embeddings, and type embeddings for differentiating between different query types. Note that position, role, and type embeddings are generated even for query types not in training data.

4.1.1 Position Embedding

Previous studies (Dwivedi et al., 2022; You et al., 2019) have shown the advantages of incorporating canonical positioning information within message-passing frameworks to present nodes in arbitrary graphs. Inspired by this, we propose incorporating the canonical positioning information in the representation of each node within the query graph, aiming to lead to a more expressive and informative representation.

To capture the relative order of nodes within a query graph, we introduce the concept of canonical node positions. These positions represent the order in which nodes would appear if the graph were listed from left to right, as illustrated in Figure 3 (the first number in each tuple). Importantly, the maximum canonical position number remains consistent across all queries of the same type and equals the maximum query length. For example, consider the $3p$ query graph in Figure 2. When listing nodes from left to right (starting with the anchor node), the maximum position is 4. Therefore, we initialize position embeddings for canonical positions 0 to 3 as follows:

$$\mathbf{P}_{pos} = [\mathbf{p}_0 \ \mathbf{p}_1 \ \mathbf{p}_2 \ \mathbf{p}_3] \in \mathbb{R}^{4 \times d_{pos}}, \quad (3)$$

where d_{pos} denotes the dimension of the position embedding, and \mathbf{p}_i represents the position embedding of a node at the i -th canonical position on the query graph. The lookup table \mathbf{P}_{pos} maps each potential canonical position i to its corresponding embedding vector \mathbf{p}_i . Then, \mathbf{p}_i is integrated into the embedding of the node located at the i -th position on the query graph. The integration of this position embedding aims to compensate for the lack of explicit structural information arising from the sequential nature of existing embedding models.

4.1.2 Role Embedding

Query graphs reveal important structural information through distinct node roles. Regardless of the type of query, anchor nodes never have incoming edges, as shown in Figure 2. In contrast, variable nodes are connected to other nodes from both incoming and outgoing edges. Finally, answer nodes serve as leaf nodes, with no outgoing edges. These distinct node roles, observed across various query graph types, offer valuable insights into the query’s structure, enriching the information available for the embedding model.

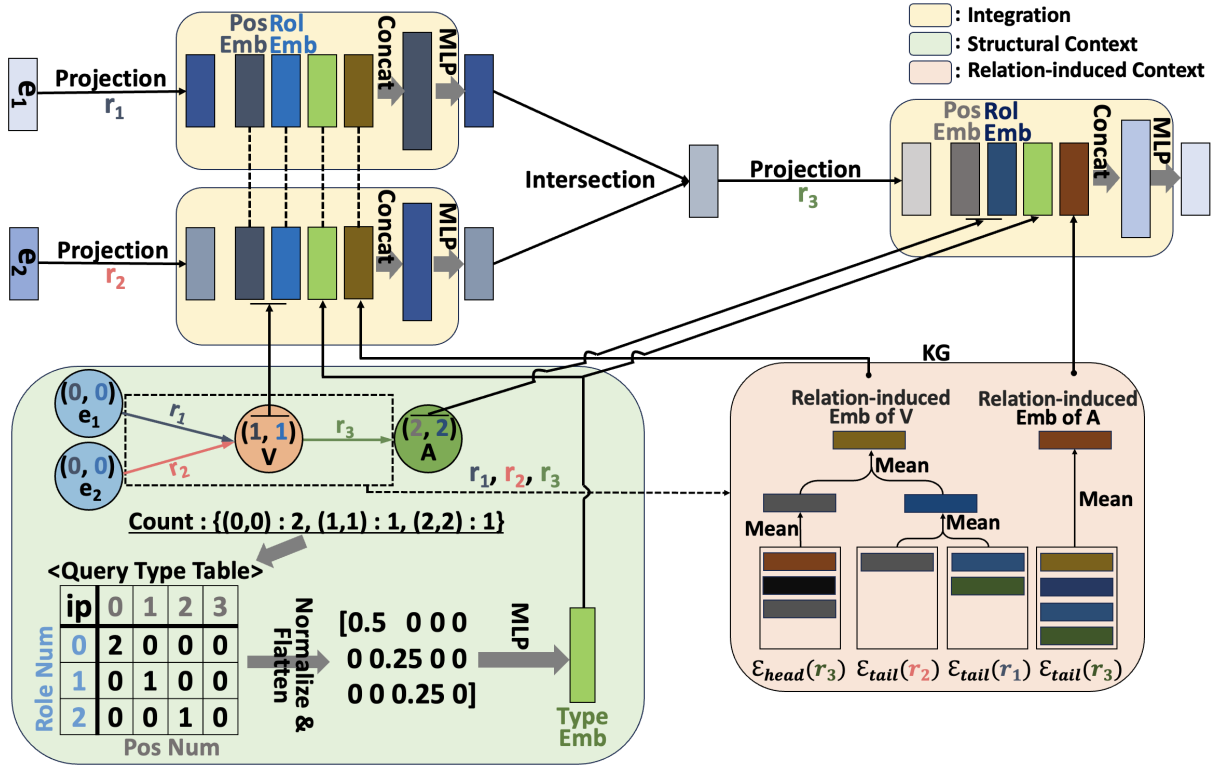


Figure 3: The figure of the structural context and relation-induced context and its application example on *ip* query. Each node in the query graph can be assigned a position number and a role number, which is represented as a tuple in the *Structural Context* box (green box). The first number of the tuple in each node of the query graph represents the *position* number, and the second number indicates the *role* number. Type embedding is derived from the query-type table containing the position and role information of the corresponding query graph. The *Relation-induced Context* box illustrates constructing relation-induced embedding of node V and A from KG. The *Integration* box describes integrating query embedding, position embedding, role embedding, type embedding, and relation-induced embedding into updated query embedding. Best viewed in color.

To take advantage of this information, we assign a canonical number to each role of the query graph (i.e., 0 for the anchor node, 1 for the variable node, 2 for the answer node) and initialize the role embedding for each role as:

$$\mathbf{R}_{rol} = [\mathbf{r}_{anch} \ \mathbf{r}_{var} \ \mathbf{r}_{ans}] \in \mathbb{R}^{3 \times d_{rol}}, \quad (4)$$

where d_{rol} represents the dimension of the role embedding. \mathbf{R}_{rol} is a lookup table containing role embeddings. \mathbf{r}_{anch} , \mathbf{r}_{var} , and \mathbf{r}_{ans} are role embeddings for anchor, variable, and answer nodes, respectively. The role embedding is incorporated into the query embeddings of the corresponding node to provide information about the node's role within the query graph.

4.1.3 Type Embedding

While position and role embeddings provide valuable information about each node within a query graph, they don't necessarily reveal the complete picture of how these nodes interact and contribute to the distinct query structures. For instance, they

may struggle to represent unique query types like $2i$ and $3i$ in Figure 2. The answer entities in both $2i$ query and $3i$ query have position 1 with respect to the anchor entity (*position 0*) and have the same role embedding (*answer*). Therefore, position embedding and role embedding are not enough to reflect the different structure information of $2i$ and $3i$ query graphs.

To address this limitation, we propose a method to capture the structural context of a given query type. This approach extends beyond individual node properties to understand the broader relationships and dependencies between them. To capture this crucial structural context, we introduce the query-type table. Illustrated in the *Structural Context* box of Figure 3, this table encodes the complete structural information of the query by representing each node as a combination of its position and role. Flattening this table results in a vector, where each element corresponds to a specific position-role combination. Consequently, this

vector uniquely identifies the query’s structure (i.e., query type). Because the range of values in the query type table is different for each query type, we normalize the vector by dividing by 4, which is the maximum sum of the values in the vector. Finally, we use a linear transformation to map this normalized vector into a continuous embedding space, creating the type embedding. For a query graph \mathcal{G} , the type embedding of any node in the query graph \mathcal{G} is presented as follows:

$$\mathbf{g}_{\mathcal{G}} = \mathbf{W}_g \cdot \text{flatten}(\text{Count}(\mathcal{G})). \quad (5)$$

Count returns a query-type table ($\text{Count}(\mathcal{G}) \in \mathbb{R}^{3 \times 4}$), constructed by counting the occurrence of each combination of position number and role number for the nodes in the graph \mathcal{G} . The flatten function transforms this two-dimensional query-type table into a vector. \mathbf{W}_g represents a linear transformation matrix. The type embedding is then incorporated into the query embedding of each node within a query graph. All nodes within a query graph share the same query table, resulting in identical type embedding. It’s worth noting that we collectively refer to the position, role, and type embeddings as *structure embeddings*.

4.2 Learning Relation-induced Context

Several approaches have been proposed for leveraging neighboring relations around entities to enhance reasoning in KGs (Sheng et al., 2020; Chen et al., 2022a). However, computing attention scores, as in (Sheng et al., 2020), requires a high computational cost, making it more expensive to apply these approaches concurrently with computing the query embedding. Additionally, it is challenging to represent an entity solely based on relations’ embedding as in (Chen et al., 2022a) due to the distinct distributions of entities and relations. To extract relation-induced context associated with the nodes, we first define $\mathcal{N}_r^{\text{in}}(v_i)$ as the set of incoming relations of the node v_i in the query graph. $\mathcal{N}_r^{\text{out}}(v_i)$ represents the set of outgoing relations of the node v_i in the query graph. We then utilize the connection of the relation in the KG to acquire the information possessed by the relation associated with node v_i on the query graph. To achieve this, we define the entities serving as the tail of relation r in the KG as $\mathcal{E}_{\text{tail}}(r)$, and the entities serving as the head as $\mathcal{E}_{\text{head}}(r)$. We then aggregate the embeddings of these entities to construct the relation-induced context of the node, referred to

as the relation-induced embedding. This can be formulated as follows:

$$\mathbf{l}_v^{\text{in}} = \text{Agg}\{\text{Emb}(e) \mid e \in \mathcal{E}_{\text{tail}}(r), r \in \mathcal{N}_r^{\text{in}}(v)\}, \quad (6)$$

$$\mathbf{l}_v^{\text{out}} = \text{Agg}\{\text{Emb}(e) \mid e \in \mathcal{E}_{\text{head}}(r), r \in \mathcal{N}_r^{\text{out}}(v)\}, \quad (7)$$

$$\mathbf{l}_v = (\mathbf{l}_v^{\text{in}} + \mathbf{l}_v^{\text{out}})/2, \quad (8)$$

where we use the mean operation as the Agg function, and \mathbf{l}_v indicates the relation-induced embedding of node v . Note that in Equation (6) and (7), considering computational efficiency, we sample up to K number of entities from $\mathcal{E}_{\text{tail}}(r)$ and $\mathcal{E}_{\text{head}}(r)$, respectively.

4.3 Integrating Two Contextual Embeddings

We incorporate the structural embedding (Sec 4.1) and the relation-induced embedding (Sec 4.2) into the embeddings of each node in the query graph using a neural network architecture. Different embeddings are passed through the neural network, concatenated, and then mapped into the same low-dimensional embedding space as the original query embedding. The node embedding of the arbitrary query graph \mathcal{G} , which incorporates the obtained information from above, can be formulated as follows:

$$\mathbf{p}_v = \mathbf{P}_{\text{pos}}[\text{position}_v], \quad (9)$$

$$\mathbf{r}_v = \mathbf{R}_{\text{rol}}[\text{role}_v], \quad (10)$$

$$\mathbf{q}'_v = \mathbf{W}' \cdot (\text{MLP}_q \cdot \mathbf{q}_v \mid \text{MLP}_I(\{\mathbf{p}_v, \mathbf{r}_v, \mathbf{g}_{\mathcal{G}}, \mathbf{l}_v\})), \quad (11)$$

where $[\cdot]$ is a lookup operation. Note that the node v can be either a variable node or an answer node in \mathcal{G} . position_v denotes the canonical position of node v in the query graph \mathcal{G} . role_v represents the number corresponding to the role of node v in the query graph \mathcal{G} . \mathbf{p}_v , \mathbf{r}_v , $\mathbf{g}_{\mathcal{G}}$, and \mathbf{l}_v represent the position embedding, role embedding, type embedding, and the relation-induced embedding of node v , respectively. MLP_q and MLP_I signify multi-layer perceptrons, respectively. $(\cdot \mid \cdot)$ is a concatenation. \mathbf{q}_v represents the embedding of the branch toward node v in the query graph resulting from projection operators of the base query embedding model (e.g., Q2B, BetaE, or ConE). \mathbf{q}'_v represents the updated representation obtained by integrating structural and relation-induced context into \mathbf{q}_v .

The query embedding models sequentially compute embeddings of nodes in the query graph, ultimately deriving the embedding for the answer

node. The integration occurs at each instance of a projection operation. The position, role, type, and relation-induced embeddings are precomputed for each variable node and answer node. During the execution of projection operation, these context embeddings are integrated into the embedding of the corresponding node in the query graph, resulting in an enhanced representation.

4.4 Training

The structure embeddings, relation-induced embedding and parameters consisting of neural networks of Equation (11) for integration are updated through backward propagation from the loss function of each query embedding model. The loss function defined in the query embedding model is common as follows:

$$L_{qe} = -\log \sigma(\gamma - \text{Dist}(\mathbf{v}, \mathbf{q}'_A)) - \sum_{j=1}^k \frac{1}{k} \log \sigma(\text{Dist}(\mathbf{v}'_j, \mathbf{q}'_A) - \gamma). \quad (12)$$

Here, \mathbf{q}'_A indicates the modified query embedding of the answer node by Equation (11). \mathbf{v} and \mathbf{v}'_j denote the positive (i.e., answer entity) and negative entity for each query. k represents the number of negative samples (Mikolov et al., 2013), and Dist is the model-specific function that measures the distance between query embedding and entity embedding.

In the case of BetaE, utilizing entities' embeddings as parameters for beta distributions can lead to significant variance shifts, hindering the convergence of the model's learning. Therefore, for BetaE, we introduce an additional loss to mitigate the variance shifts. The details about the variance loss are provided in Appendix D.

4.5 Time Complexity Analysis

Acquiring the relation-induced embedding costs $\mathcal{O}(NKD)$, where N is the number of nodes in the query graph, K is the size of sample entities for constructing the relation-induced embedding, and D is the dimension of the embedding. When integrating all embeddings, $\mathcal{O}(PMD^2 + NKD) \approx \mathcal{O}(1 \cdot D^2)$ is required. Here, P is the number of projection operations in the given query, and M is the number of contextual information embeddings used (4 in case when using all embeddings). In addition to the analysis, we compare the inference times of the query embedding model and that with our methodology in Table 4 of Appendix.

5 Experiments

5.1 Datasets and Base Reasoning Models

For evaluation, we use two datasets: FB15k-237 (Toutanova and Chen, 2015) and NELL (Xiong et al., 2017). We evaluate the effectiveness of our approach on the Q2B (Ren et al., 2020), BetaE (Ren and Leskovec, 2020), and ConE (Zhang et al., 2021) models, which have received considerable attention in various FOL tasks as foundation models. For more detailed information on the datasets and query structures, please refer to Appendix A.

5.2 Main Results

Table 1 demonstrates that applying our method results in performance gains for all compared models, with Q2B showing a particularly notable 19.5% increase on the NELL dataset. This significant improvement could stem from the unique alignment between Q2B's hyper-rectangular embedding space and the space where our position, role, and type embeddings are mapped.

The lower performance of BetaE+CaQR(R) compared to BetaE+CaQR(S) can be attributed to the parameters of BetaE. BetaE utilizes two d-dimensional embedding vectors, α and β , as the parameters of beta distributions, to represent entities. The relation-induced embedding is constructed for each query node by computing the average values across multiple entities. However, since the parameter of averaged multiple beta distributions is not the same as the average of parameters of beta distributions, the resulting relation-induced embedding can deviate from the actual values.

While not as pronounced as with Q2B and BetaE, our method still delivers performance gains for ConE across 1p, 2p, and 3p queries. This suggests that our methodology benefits even simpler query structures, indicating its broad applicability and effectiveness. Table 1 demonstrates a consistent performance improvement with the application of CaQR(S). Furthermore, in the context of complex queries (e.g., $2i$, $3i$, pi , and ip), a synergistic effect is evident when both S and R are employed.

Table 2 presents the experimental results for queries with negation. While there is an overall positive effect, it is smaller compared to previous query types. This could be attributed to the late application of our method, which operates after the projection step.

Dataset	Model	1p	2p	3p	2i	3i	pi	ip	2u	up	Avg	Imp(%)
FB15k-237	Q2B	40.35	9.27	6.87	28.57	40.88	20.71	12.75	10.96	7.48	19.76	-
	Q2B+CaQR(S)	42.49	10.82	8.92	32.55	45.92	23.44	13.29	14.27	8.67	22.26	12.7
	Q2B+CaQR(R)	42.66	10.94	9.18	32.53	45.98	22.00	13.47	14.46	8.45	22.18	12.2
	Q2B+CaQR	42.65	10.82	9.00	32.43	46.42	21.70	13.39	14.53	8.75	22.19	12.3
	BetaE	39.20	10.69	10.15	29.16	42.59	22.53	12.28	12.52	9.73	20.98	-
	BetaE+CaQR(S)	40.82	12.16	10.78	32.04	45.80	24.66	13.71	13.94	10.59	22.72	8.3
	BetaE+CaQR(R)	41.08	12.31	10.70	31.64	45.21	24.49	14.22	13.94	10.46	22.67	8.1
	BetaE+CaQR	41.35	12.75	10.79	31.89	45.55	24.70	14.69	14.24	10.67	22.96	9.4
	ConE	42.33	12.78	10.97	32.59	47.13	25.45	13.71	14.35	10.50	23.31	-
	ConE+CaQR(S)	42.89	13.13	11.16	33.07	47.56	24.75	11.97	15.49	10.90	23.44	0.5
	ConE+CaQR(R)	42.92	12.98	11.16	32.32	46.99	24.31	14.36	15.18	10.67	23.43	0.5
	ConE+CaQR	41.81	12.84	10.90	33.78	48.24	25.65	14.41	14.48	10.95	23.67	1.5
NELL	Q2B	41.48	13.80	11.17	32.01	44.71	21.90	16.80	11.19	10.12	22.57	-
	Q2B+CaQR(S)	57.12	16.15	13.54	37.81	50.92	23.45	17.47	14.60	10.37	26.83	18.9
	Q2B+CaQR(R)	57.15	16.08	13.75	37.84	50.68	22.82	18.03	14.80	10.36	26.83	18.9
	Q2B+CaQR	57.15	15.99	13.42	37.95	51.25	24.24	17.57	14.80	10.42	26.97	19.5
	BetaE	53.09	13.10	11.56	37.62	47.87	24.40	14.89	12.05	8.63	24.80	-
	BetaE+CaQR(S)	54.72	14.83	12.58	37.49	48.34	24.06	15.00	12.50	9.76	25.47	2.7
	BetaE+CaQR(R)	54.42	14.44	12.53	37.03	47.76	24.01	15.64	12.08	9.48	25.26	1.9
	BetaE+CaQR	55.20	15.44	13.52	37.99	48.47	25.45	16.59	13.06	10.26	26.22	5.7
	ConE	53.19	16.08	14.04	39.88	51.08	26.04	17.58	15.41	11.24	27.17	-
	ConE+CaQR(S)	55.86	17.27	14.95	39.84	50.91	24.77	17.76	14.86	11.95	27.58	1.5
	ConE+CaQR(R)	55.28	16.94	14.77	39.95	50.98	24.31	16.42	15.02	11.41	27.23	0.2
	ConE+CaQR	56.05	17.49	14.57	40.46	51.08	22.99	16.50	15.06	11.99	27.35	0.7

Table 1: MRR results (%) for answering conjunctive queries without negation (\exists , \wedge , \vee) on FB15k-237 and NELL. *Imp* denotes the percentage of improvement in average MRR compared to the base reasoning models. +CaQR(S) denotes the model utilizing structure embedding. +CaQR(R) indicates the model using relation-induced embedding. +CaQR represents the model using both structure and relation-induced embeddings. The bold text highlights the best result for each type of query.

Dataset	Model	2in	3in	inp	pni	pin	Avg	
FB15k-237	BetaE	5.19	7.94	7.44	3.60	3.55	5.54	
	BetaE+CaQR(S)	5.29	8.35	7.77	3.51	3.90	5.76	
	BetaE+CaQR(R)	5.42	8.30	7.83	3.60	3.89	5.81	
	BetaE+CaQR	5.49	8.24	8.01	3.77	3.91	5.88	
	ConE	5.78	9.57	7.95	3.85	4.41	6.31	
	ConE+CaQR(S)	6.25	9.62	7.60	3.97	4.03	6.30	
	ConE+CaQR(R)	6.84	10.44	7.66	4.49	4.79	6.85	
	ConE+CaQR	5.24	8.91	8.07	3.51	3.90	5.93	
	NELL	BetaE	5.23	7.64	10.12	3.27	3.09	5.87
		BetaE+CaQR(S)	5.37	7.96	10.43	3.46	3.29	6.10
BetaE+CaQR(R)		4.91	7.63	10.06	3.17	3.02	5.76	
BetaE+CaQR		5.50	7.62	10.87	3.70	3.30	6.20	
ConE		5.70	8.01	10.96	3.83	3.58	6.40	
ConE+CaQR(S)		6.02	8.11	11.54	4.01	3.72	6.88	
ConE+CaQR(R)		6.10	8.35	11.02	4.07	3.65	6.64	
ConE+CaQR		5.77	8.01	11.12	3.87	3.66	6.49	

Table 2: MRR results (%) for answering conjunctive queries with negation.

5.3 Ablation Study

We conduct an ablation experiment on Q2B, BetaE, and ConE to dissect the roles of position, role, and type embeddings in building the structural context of the query graph, as shown in Figure 4. Interestingly, the results reveal that using any single embedding (position, role, or type) achieves performance comparable to using the combination of all three, demonstrating the effectiveness of each embedding option.

5.4 Hyper-parameter Sensitivity Study

Two considerations arise when applying our methodology, CaQR, to a query embedding-based model: the number of entities sampled to construct the relation-induced embedding and the dimension of the structure embedding.

Size of Entity Samples. We evaluate the effect of entity samples per relation when constructing relation-induced embedding from KG on Q2B+CaQR(R). The number of entity samples varies to 60, 120, 240, and 480. The results are depicted in Figure 5 (a). For FB15k-237, we observe an improvement in performance on Q2B as the sample size increases, along with a notable variation in performance based on sample size. However, in the case of NELL, it is evident that the model’s performance is relatively insensitive to the number of samples. The number of entities on the NELL dataset could be the factor of this result because the FB15k-237 dataset has a smaller number of entities than the NELL dataset.

Dimension of Structure Embeddings. Furthermore, we conduct a hyper-parameter sensitivity study on Q2B+CaQR(S), specifically focusing on

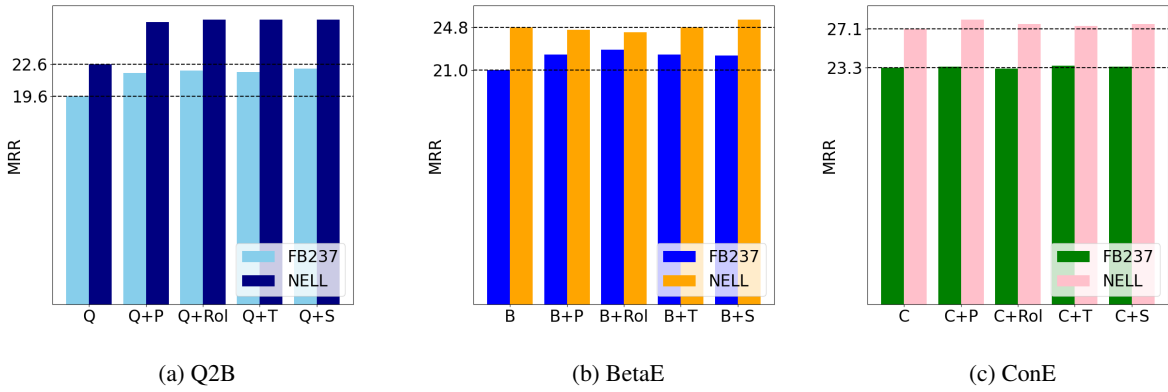


Figure 4: Ablation study on the existence of Position, Role, and Type embedding. FB237 denotes the FB15k-237 dataset. +P, +Rol, +T and +S indicates the model with position embedding, role embedding, type embedding, and all the structure embeddings, respectively.

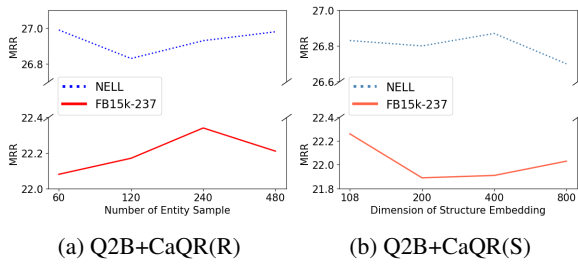


Figure 5: Effect of Hyper-parameters on Q2B+{CaQR(S), CaQR(R)}.

the effect of position embedding, role embedding, and type embedding (i.e., structure embedding) dimensions. The dimensions are varied to 108, 200, 400, and 800, respectively. The results are presented in Figure 5 (b). For FB15k-237, the most optimal performance was observed with a dimension of 108 while significant performance degradation was evident with other dimensions. In the case of NELL, it is evident that the model’s performance is relatively insensitive to changes in dimension.

6 Conclusion

In this paper, we introduced CaQR, a model-agnostic approach that leverages structural and relation-induced context within the query graph. By seamlessly fusing position, role, type, and relation-induced embeddings into the query representation, CaQR substantially improves the performance of query embedding-based multi-hop reasoning models across diverse query types.

7 Ethics Statement

Our model proposes a methodology that enhances the effectiveness of multi-hop logical reasoning by fully integrating the context of the FOL query graph. We do not additionally leverage any ex-

ternal knowledge or information that might bias the evaluation of our model. However, while this approach can improve model performance, it may also inadvertently reinforce existing harmful biases in the knowledge graphs.

8 Limitation

With the two context modeling approaches, we have observed an increase in performance. Although these approaches are model-agnostic, they may offer relatively smaller improvements, similar to those seen in ConE. Moreover, they introduce additional hyperparameters, such as the dimensions of structure and relation-induced embeddings, which can result in 1-2% fluctuation in Mean Reciprocal Rank (MRR).

9 Acknowledgement

This work was supported by the Institute of Information & Communications Technology Planning & Evaluation (IITP) grant funded by the Korea government (MSIT): (No. 2019-0-00421, Artificial Intelligence Graduate School Program (Sungkyunkwan University)) and (No. RS-2023-00225441, Knowledge Information Structure Technology for the Multiple Variations of Digital Assets). This research was also supported by the Culture, Sports, and Tourism R&D Program through the Korea Creative Content Agency grant funded by the Ministry of Culture, Sports and Tourism in 2024 (Project Name: Research on neural watermark technology for copyright protection of generative AI 3D content, RS-2024-00348469, 25%)

References

- Mingyang Chen, Wen Zhang, Yushan Zhu, Hongting Zhou, Zonggang Yuan, Changliang Xu, and Huajun Chen. 2022a. [Meta-knowledge transfer for inductive knowledge graph embedding](#). In *Proceedings of the 45th International ACM SIGIR Conference on Research and Development in Information Retrieval, SIGIR 2022, Madrid, Spain, July 11 - 15, 2022*, pages 927–937.
- Xuelu Chen, Ziniu Hu, and Yizhou Sun. 2022b. [Fuzzy logic based logical query answering on knowledge graphs](#). In *Proceedings of the 36th Association for the Advancement of Artificial Intelligence, AAAI 2022, Virtual Event, February 22 - March 1, 2022*, pages 3939–3948.
- Narendra Choudhary, Nikhil Rao, Sumeet Katariya, Karthik Subbian, and Chandan K. Reddy. 2021. [Probabilistic entity representation model for reasoning over knowledge graphs](#). In *Advances in Neural Information Processing Systems 34: Annual Conference on Neural Information Processing Systems 2021, NeurIPS 2021, December 6-14, 2021, Virtual Event*, pages 23440–23451.
- Vijay Prakash Dwivedi, Anh Tuan Luu, Thomas Laurent, Yoshua Bengio, and Xavier Bresson. 2022. [Graph neural networks with learnable structural and positional representations](#). In *The 10th International Conference on Learning Representations, ICLR 2022, Virtual Event, April 25-29, 2022*.
- William L. Hamilton, Payal Bajaj, Marinka Zitnik, Dan Jurafsky, and Jure Leskovec. 2018. [Embedding logical queries on knowledge graphs](#). In *Advances in Neural Information Processing Systems 31: Annual Conference on Neural Information Processing Systems, NeurIPS 2018, December 3-8, 2018, Montréal, Canada*, pages 2030–2041.
- Tingting Liang, Yuanqing Zhang, Qianhui Di, Congying Xia, Youhui Li, and Yuyu Yin. 2023. [Contrastive box embedding for collaborative reasoning](#). In *Proceedings of the 46th International ACM SIGIR Conference on Research and Development in Information Retrieval, SIGIR 2023, Taipei, Taiwan, July 23-27, 2023*, pages 38–47.
- Lihui Liu, Boxin Du, Heng Ji, ChengXiang Zhai, and Hanghang Tong. 2021. [Neural-answering logical queries on knowledge graphs](#). In *Proceedings of the 27th ACM SIGKDD Conference on Knowledge Discovery and Data Mining, KDD 2021, Virtual Event, Singapore, August 14-18, 2021*, pages 1087–1097.
- Tomás Mikolov, Kai Chen, Greg Corrado, and Jeffrey Dean. 2013. [Efficient estimation of word representations in vector space](#). In *The 1st International Conference on Learning Representations, ICLR 2013, Scottsdale, Arizona, USA, May 2-4, 2013, Workshop Track Proceedings*.
- Gabriel Peyré and Marco Cuturi. 2019. [Computational optimal transport: With applications to data science](#). *Foundations and Trends® in Machine Learning*, 11(5-6):355–607.
- Hongyu Ren, Weihua Hu, and Jure Leskovec. 2020. [Query2box: Reasoning over knowledge graphs in vector space using box embeddings](#). In *The 8th International Conference on Learning Representations, ICLR 2020, Addis Ababa, Ethiopia, April 26-30, 2020*.
- Hongyu Ren and Jure Leskovec. 2020. [Beta embeddings for multi-hop logical reasoning in knowledge graphs](#). In *Advances in Neural Information Processing Systems 33: Annual Conference on Neural Information Processing Systems 2020, NeurIPS 2020, December 6-12, 2020, Virtual Event*, volume 33, pages 19716–19726.
- Jiawei Sheng, Shu Guo, Zhenyu Chen, Juwei Yue, Lihong Wang, Tingwen Liu, and Hongbo Xu. 2020. [Adaptive Attentional Network for Few-Shot Knowledge Graph Completion](#). In *Proceedings of the 2020 Conference on Empirical Methods in Natural Language Processing, EMNLP 2020*, pages 1681–1691.
- Arnab Sinha, Zhihong Shen, Yang Song, Hao Ma, Darin Eide, Bo-June Paul Hsu, and Kuansan Wang. 2015. [An overview of microsoft academic service \(MAS\) and applications](#). In *Proceedings of the 24th International Conference on World Wide Web Companion, WWW 2015, Florence, Italy, May 18-22, 2015 - Companion Volume*, pages 243–246.
- Zhenwei Tang, Griffin Floto, Armin Toroghi, Shichao Pei, Xiangliang Zhang, and Scott Sanner. 2023. [Logi-crec: Recommendation with users’ logical requirements](#). In *Proceedings of the 46th International ACM SIGIR Conference on Research and Development in Information Retrieval, SIGIR 2023, Taipei, Taiwan, July 23-27, 2023*, pages 2129–2133.
- Kristina Toutanova and Danqi Chen. 2015. [Observed versus latent features for knowledge base and text inference](#). In *Proceedings of the 3rd Workshop on Continuous Vector Space Models and their Compositionality*, pages 57–66, Beijing, China.
- Denny Vrandečić and Markus Krötzsch. 2014. [Wiki-data: a free collaborative knowledgebase](#). *Commun. ACM*, 57(10):78–85.
- Zihao Wang, Weizhi Fei, Hang Yin, Yangqiu Song, Ginny Y. Wong, and Simon See. 2023a. [Wasserstein-fisher-rao embedding: Logical query embeddings with local comparison and global transport](#). In *Findings of the Association for Computational Linguistics, ACL 2023, Toronto, Canada, July 9-14, 2023*, pages 13679–13696.
- Zihao Wang, Yangqiu Song, Ginny Y. Wong, and Simon See. 2023b. [Logical message passing networks with one-hop inference on atomic formulas](#). In *The 11th International Conference on Learning Representations, ICLR 2023, Kigali, Rwanda, May 1-5, 2023*.

- Bo Xiong, Mojtaba Nayyeri, Ming Jin, Yunjie He, Michael Cochez, Shirui Pan, and Steffen Staab. 2023. [Geometric relational embeddings: A survey](#). *CoRR*, abs/2304.11949.
- Wenhan Xiong, Thien Hoang, and William Yang Wang. 2017. [Deeppath: A reinforcement learning method for knowledge graph reasoning](#). In *Proceedings of the 2017 Conference on Empirical Methods in Natural Language Processing, EMNLP 2017, Copenhagen, Denmark, September 9-11, 2017*, pages 564–573.
- Yao Xu, Shizhu He, Cunguang Wang, Li Cai, Kang Liu, and Jun Zhao. 2023. [Query2triple: Unified query encoding for answering diverse complex queries over knowledge graphs](#). In *Findings of the Association for Computational Linguistics, EMNLP 2023, Singapore, December 6-10, 2023*, pages 11369–11382.
- Dong Yang, Peijun Qing, Yang Li, Haonan Lu, and Xiaodong Lin. 2022. [Gammae: Gamma embeddings for logical queries on knowledge graphs](#). In *Proceedings of the 2022 Conference on Empirical Methods in Natural Language Processing, EMNLP 2022, Abu Dhabi, United Arab Emirates, December 7-11, 2022*, pages 745–760.
- Jiaxuan You, Rex Ying, and Jure Leskovec. 2019. [Position-aware graph neural networks](#). In *Proceedings of the 36th International Conference on Machine Learning, ICML 2019, 9-15 June 2019, Long Beach, California, USA*, volume 97 of *Proceedings of Machine Learning Research*, pages 7134–7143.
- Zhanqiu Zhang, Jie Wang, Jiajun Chen, Shuiwang Ji, and Feng Wu. 2021. [Cone: Cone embeddings for multi-hop reasoning over knowledge graphs](#). In *Advances in Neural Information Processing Systems 34: Annual Conference on Neural Information Processing Systems 2021, NeurIPS 2021, December 6-14, 2021, Virtual Event*, pages 19172–19183.
- Zhaocheng Zhu, Mikhail Galkin, Zuobai Zhang, and Jian Tang. 2022. [Neural-symbolic models for logical queries on knowledge graphs](#). In *International Conference on Machine Learning, ICML 2022, 17-23 July 2022, Baltimore, Maryland, USA*, volume 162 of *Proceedings of Machine Learning Research*, pages 27454–27478.

A Experimental Details

We use the default parameters from the existing baseline. The hyperparameter search was conducted for the number of entity samples {60, 120, 240, 480} and for the dimension of the structure embedding {108, 200, 400, 800}. We use 120 for the entity sample size, 800 for structure embedding for ConE (Zhang et al., 2021), and 108 for the other baselines.

A.1 Datasets

We use two datasets to study CaQR :

- FB15k-237 (Toutanova and Chen, 2015) consists of 14,505 entities, 237 relations, and 272,115 triplets when not considering the inverse of relations. In the process of obtaining relation-induced context information from the query graph, we utilize 544,230 triplets considering the inverse of relations.
- NELL (Xiong et al., 2017) comprises 63,361 entities, 400 relations, and 114,213 edges without considering the inverse of relations. We utilize 228,426 triplets considering the inverses when obtaining relation-induced context information from the query graph.

A.2 Query Dataset

The query data employed for the experiment comprises 14 types as illustrated in Figure 6 with 4 of them (i.e., *ip*, *pi*, *2u*, and *up*) exclusively utilized for evaluation purposes. The statistics of the query data are provided in Table 3.

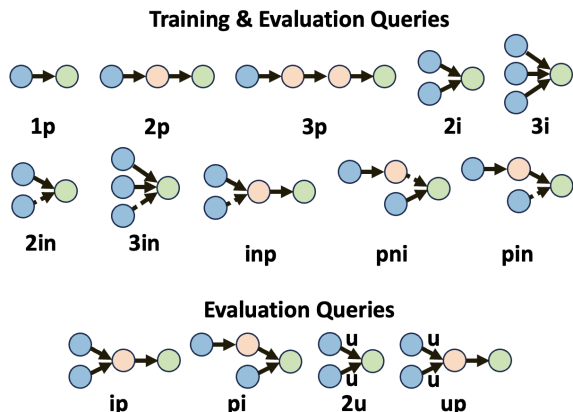


Figure 6: Query types used in experiments.

A.3 Base Reasoning Models

Since our approach is model-agnostic, it can be applied to any query embedding-based multi-hop

Table 3: The Statistics of Query Datasets. Neg. means queries with negation operators.

Dataset	Training		Validation		Test	
	w/o Neg.	Neg.	1p	others	1p	others
FB15k-237	273,710	27,371	59,078	8,000	66,990	8,000
NELL	149,689	14,968	20,094	5,000	22,804	5,000

reasoning model. Therefore, we evaluate the effectiveness of our approach on the Q2B (Ren et al., 2020), BetaE (Ren and Leskovec, 2020), and ConE (Zhang et al., 2021) models for conjunctive query types with path lengths 1, 2, and 3 (*1p*, *2p*, *3p*, *2i*, *3i*, *2in*, *3in*, *inp*, *pni*, *pin*, *ip*, *pi*, *2u*, and *up*). Note that evaluations involving negations (*2in*, *3in*, *inp*, *pni*, and *pin*) are excluded on Q2B due to their limitations of the inability to address negations.

B Computation Graph

The computation graph shows a computationally feasible form of query graph using logical operators. Each query graph can be mapped into its corresponding computation graph (Ren et al., 2020), where each atomic formula is represented with relation projection, merged by intersection, and transformed negation by complement. The computation graph effectively demonstrates the computational procedure to resolve the query. In a computation graph, each node represents an embedding or a distribution over a set of entities in the KG, and each edge signifies a logical transformation (e.g., relational projection, intersection/union/negation operators) of this distribution. The computation graph for a FOL query resembles a tree. The root node of the computation graph represents the answer (or target) variable, with one or more anchor nodes provided by the FOL. Embeddings of entities and transformation operators are initialized; embeddings of anchor nodes are then input into the connected neural network of logical operators in a serial manner to obtain the final embeddings for the answer variable, thereby creating a query embedding. During training, models ensure the proximity of query embeddings to the ground truth. In the prediction stage, entities close to the query embedding are utilized for prediction. We follow the original implementations of the base reasoning models, such as Q2B, BetaE, and ConE. Four logical operators are used to express the first-order logic queries: relation projection operator, intersection operator, union operator, and negation operator.

- **Relation projection operator.** For a set of

entities $S \subseteq \mathcal{V}$, and a relation type $r \in \mathcal{R}$, the relation projection operator produces all the neighboring entities $\cup_{v \in S} N(v, r)$, where $N(v, r) \equiv \{v' \in \mathcal{V} \mid r(v, v') = True\}$.

- **Intersection operator.** For a set of entity sets, $\{S_1, S_2, \dots, S_n\}$ of size n , the intersection operator outputs $\cap_{i=1}^n S_i$.
- **Union operator.** Given a set of entity sets, $\{S_1, S_2, \dots, S_n\}$ of size n , the union operator produces $\cup_{i=1}^n S_i$.
- **Negation operator.** The negation operator outputs a complement set, $\bar{S} \equiv \mathcal{V} \setminus S$, of a set of entities $S \subseteq \mathcal{V}$.

C Case Study

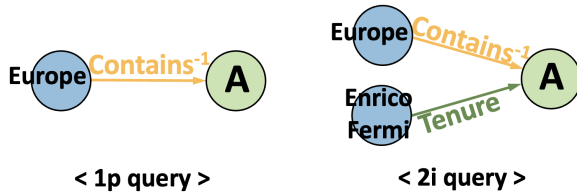


Figure 7: 1p query and 2i query.

To investigate whether our model reflects the context of the query graph in its embeddings, we conduct a case study using the 1p query $Contains^{-1}(Europe, A)$ and the 2i query $Contains^{-1}(Europe, A) \wedge Tenure(Enrico, A)$ (Figure 7). When employing the conventional query embedding (Q2B) approach, it is not possible to capture the overall context of the query graph, thus resulting in the same query embedding for the $Contains^{-1}(Europe, A)$ in 1p and 2i queries. On the contrary, when applying our model, we observe the difference between $Contains^{-1}(Europe, A)$ embedding of 1p and 2i query indicating the incorporation of the query graph’s context into the embeddings.

As shown in Figure 8a, through Q2B, it is impossible to obtain embedding that reflects the query graph context. Consequently, around the embedding of the $Contains^{-1}(Europe, A)$ branch (black), entities unrelated to the branch $Tenure(EnricoFermi, A)$, which are not in the domain of *University* are mapped in close proximity. Conversely, upon applying our model, as depicted in Figure 8b, an adaptation based on the context of the query graph becomes apparent. The embedding of the

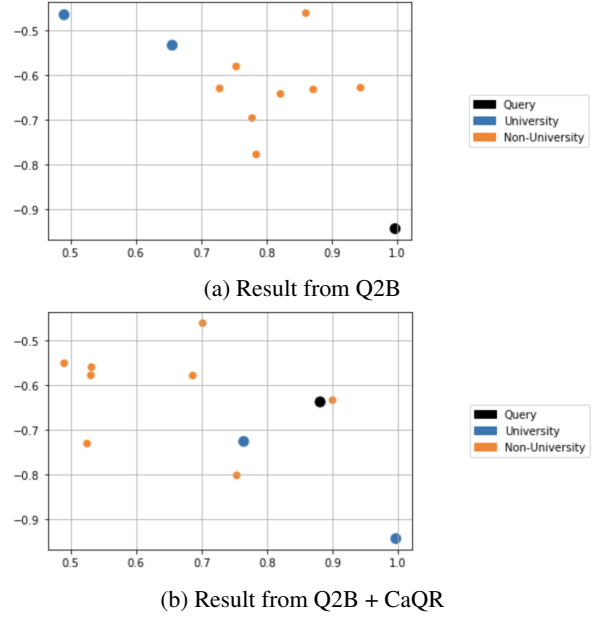


Figure 8: The embedding results of two models for a branch $Contains^{-1}(Europe, A)$ in the 2i query.

$Contains^{-1}(Europe, A)$ branch (black) is influenced by the $Tenure(EnricoFermi, A)$ branch, leading to entities associated with *University* close to the query embedding. This case shows the capacity to obtain refined representations by incorporating query context, yielding more accurate answers.

D Variance Loss

Our approach ensures that the centers of query embedding, whether they are central points within the coordinate system, the averages of probability distributions, or the central axis of a cone in a polar coordinate, experience nuanced adjustments based on the contextual information inherent to the query. This leads to an enhanced representation by integrating both the overall structural and the relation-induced context within the query graph. However, the probability-based query embedding approach, such as BetaE (Ren and Leskovec, 2020), employs parameters (α, β) of multiple beta distributions as query embeddings. In this method, when the embedding changes, it not only affects the centers but also alters the variances. Consequently, to mitigate unintended shifts in variance hindering the convergence of a model, we introduce a variance loss to BetaE. The adjusted embedding, q'_A , does not deviate significantly from the offset of the query embedding composed of the parameters learned by

the BetaE, \mathbf{q}_A , as follows:

$$\mathcal{L}_{var} = \|\text{Var}(\mathbf{q}_A) - \text{Var}(\mathbf{q}'_A)\|_2, \quad (13)$$

where $\text{Var}(\cdot)$ returns a vector of variances of beta distributions consisting of Beta embedding. The loss considering Equation (13) is as follows:

$$\mathcal{L} = \mathcal{L}_{qe} + \lambda \mathcal{L}_{var}, \quad (14)$$

where the λ is a hyper-parameter that determines the weighting of the variance loss. Details about Equation (13) are provided in Appendix A. Detailed formula of Equation (13) can be written as follow:

$$\mathbf{q}_A = [(\alpha_1, \beta_1), \dots, (\alpha_d, \beta_d)], \quad (15)$$

$$\mathbf{q}'_A = [(\alpha'_1, \beta'_1), \dots, (\alpha'_d, \beta'_d)]. \quad (16)$$

Here, \mathbf{q}_A and \mathbf{q}'_A are embedding learned by the BetaE, and adjust query embedding of answer node A of query graph, as described in Section 4.4 of the main text. d is the dimension of BetaE, the number of beta distributions representing the query. When $Beta_i$ is a beta distribution parameterized by α_i and β_i , variance of \mathbf{q}_A and \mathbf{q}'_A are as follow:

$$\text{Var}(\mathbf{q}_A) = [\sigma(Beta_1), \dots, \sigma(Beta_d)] \quad (17)$$

$$\text{Var}(\mathbf{q}'_A) = [\sigma(Beta'_1), \dots, \sigma(Beta'_d)], \quad (18)$$

where $\sigma(\cdot)$ is a variance of a probability distribution, and

$$\sigma(Beta_i) = \frac{\alpha_i \beta_i}{(\alpha_i + \beta_i)^2 (\alpha_i + \beta_i + 1)}, \quad (19)$$

$$\sigma(Beta'_i) = \frac{\alpha'_i \beta'_i}{(\alpha'_i + \beta'_i)^2 (\alpha'_i + \beta'_i + 1)}. \quad (20)$$

Then, we add the L2 norm of variance difference between the query embedding constructed with pre-trained BetaE and the adjusted query embedding to the query-answering loss as described in Equation (14) with coefficient λ .

E Inference Time Comparison

We evaluate the inference times of both the baseline and the baseline with our methodology applied, showcasing the outcomes in Table 4.

F Further Experiment

In addition to experiments conducted on Q2B, BetaE, and ConE, we further performed experiments applying our CaQR to the FuzzQE (Chen et al., 2022b) using the FB15k-237 dataset. The experimental results are on the Table 5. We observe performance improvements even for FuzzQE.

Model	Inference Time (ms)		
	$3p$	$3i$	ip
Q2B	2.0 (\pm 1.6)	2.3 (\pm 1.3)	2.6 (\pm 1.9)
Q2B + CaQR(S)	3.3 (\pm 2.3)	2.9 (\pm 2.5)	3.8 (\pm 2.7)
Q2B + CaQR(R)	5.4 (\pm 4.3)	3.4 (\pm 2.4)	3.6 (\pm 1.5)
Q2B + CaQR	9.6 (\pm 6.9)	4.6 (\pm 3.2)	6.5 (\pm 4.7)

Table 4: Averages and standard deviations of inference time on 1,000 queries involving complex query types ($3p$, $3i$, ip). CaQR(S) denotes the model with position, role, and type embedding. CaQR(R) indicates the model with relation-induced embedding.

Table 5: MRR results (%) of applying CaQR to FuzzQE on FB15k-237 dataset. Avg_P, Avg_N, and Avg represent the average results for query types without negation, query types with negation, and all query types, respectively.

Model	Avg_P	Avg_N	Avg	Imp(%)
FuzzQE	21.19	6.91	16.09	-
FuzzQE+CaQR	23.10	7.13	17.39	8.1